A comparison of the rank of different products to the color of the sample (Table III) is interesting. The four products that were found to be the purest, including the nitrates, were products corresponding to screening design numbers 1, 3, 9, and 12. These are the only four compounds to exhibit a green color (Table III). This may suggest that the desired color of the Cu/Cr LDHs tends to be a green rather than brown or black. The color of the CuCr LDH powder may be another indicator of the purity of the Cu/Cr LDH. The separate Cu/Al LDH and Zn/Cr LDH materials are blue and lavender, respectively, suggesting there is an electronic interaction between Cu^{2+} and Cr^{3+} ions in Cu/Cr LDH. Since a range of colors exist for the Cu/Cr LDHs prepared here, it is likely that different degrees of interaction between Cu^{2+} and Cr^{3+} ions exist in these materials. Our results are specific for the preparation of Cu/Cr LDH and are not expected to be applied universally for all LDH compounds. Similar conclusions regarding the nonstandardized conditions for preparations of specific combinations of cations in LDHs have also been reached by others.[14-17]

Conclusions

These results of this study clearly show that screening design experiments can be used to determine the factors of major importance in preparing Cu/Cr LDH materials. Thermogravimetric, EPR, and XRD techniques were used to evaluate the 12 synthesized products for purity, Cu^{2+} and Cr^{3+} interactions, and crystallinity. The apparent importance of the cation of the hydroxide (NaOH or KOH) was unexpected and will be interesting to examine in future work. Also, the lack of importance of some variables such as drip rate and atmosphere was unexpected. This suggests that kinetics of mixing and carbonate impurities are not as important in the Cu/Cr LDH system as one would expect. Results of the screening design suggest that the Cu/Cr LDH system is far from being completely understood and that small changes in synthetic parameters may result in large changes in the prepared product. Also, LDH systems other than Cu/Cr may have their own synthetic preferences which need to be explored and discovered to optimize the purity and desired properties of these LDHs. Further studies are underway to establish relationships among the most important synthetic variables determined in this study. The electronic properties of these Cu/Cr systems are under investigation in our laboratories.

Acknowledgment. We acknowledge the support of the National Science Foundation Grant Program under Grant CBT 8814974, the State of Connecticut Department of Higher Education, and the University of Connecticut for support of this research.

$LiMoN_2$: The First Metallic Layered Nitride

S. H. Elder, Linda H. Doerrer, and F. J. DiSalvo*

Department of Chemistry, Baker Laboratory Cornell University, Ithaca, New York 14853-1301

J. B. Parise

Mineral Physics Institute, State University of New York at Stony Brook, Stony Brook, New York 11794

D. Guyomard and J. M. Tarascon

Bell Communications Research, 311 Newman Springs Rd., Redbank, New Jersey 07701

Received March 27, 1992. Revised Manuscript Received June 5, 1992

We report the first example of a layered ternary lithium nitride in which the lithium can be deintercalated and reintercalated. The synthesis of $LiMoN_2$ is also the first example of a ternary nitride formed from either the ammonolysis of a molecular organometallic molecule, $Li_2Mo(N^tBu)_4$ or the ammonolysis of a ternary oxide, Li_2MoO_4. Elucidation of the unique structure, in a classic illustration, required both synchrotron X-ray and neutron diffraction data. The space group is $R3$ with lattice parameters (Å; from the neutron data) of $a = 2.8674$ (2) and $c = 15.801$ (2). The ideal structure consists of MoN_2 layers with Mo in trigonal prismatic holes and Li in octahedral holes between the MoN_2 layers. The presence of cation anti-site defects was clearly indicated by the joint X-ray/neutron data refinement; the structure is best described as $(Li_{0.85}Mo_{0.15})_{oct}(Mo_{0.85}Li_{0.15})_{tp}N_2$. $LiMoN_2$ is Pauli paramagnetic with $\chi_0 = 0.59 \times 10^{-6}$ emu g^{-1}. We have employed a variety of different oxidizing agents for the deintercalation of the lithium from $LiMoN_2$ and have been able to deintercalate up to 64% of the lithium. This deintercalated species can be reintercalated with *n*-butyllithium at room temperature. In contrast, electrochemical studies show a large hysteresis in the charge/discharge cycles with no reversibility.

Introduction

Since the discovery of high-T_c superconducting oxides, literally thousands of research groups worldwide have been investigating them in order to quantify their structural and physical properties, as well as attempting to improve their superconducting behavior. We are searching for families of compounds other than oxides that will exhibit this phenomenon. We have chosen to focus on ternary (or higher) nitrides since "N^{3-}" is most similar to O^{2-} with respect to size, polarizability, and electronegativity. Also, and perhaps more importantly, little work has been done

* To whom correspondence should be addressed.

0897-4756/92/2804-0928$03.00/0

on anything more complicated than the binary nitrides with the exception of lithium--rich ternary nitrides. The structures of these latter compounds are ordered variants of anti-CaF_2, and all are electrical insulators.[1-3] Consequently, these are unlikely candidates for superconductors. Thus, possible connections to superconductivity and the lack of previous work have prompted us to search for new and potentially exciting compounds in the ternary nitrides.

We and others have not been disappointed in the quest for new nitrides. Recent work has produced numerous alkaline- and alkaline-earth-metal–transition-metal nitrides with interesting chemical, structural, and physical properties: MNiN (M = Ca, Sr or Ba),[4,5] Ca_3MN (M = P, As, Sb, Bi, Ge, Sn, Pb),[6] $MTaN_2$ (M = Na, K, Rb, Cs),[7] Ca_3CrN_3,[8] Ca_6MN_5 (M = Ga and Fe),[9] Ba_3MN_4 (M = Mo and W),[10] Ba_3FeN_3,[11] and $M_2LiFe_2N_3$ (M = Sr and Ba).[12]

Nitrides have small free energies of formation due in part to the strong triple bond in dinitrogen (225 kcal/mol). The synthesis of such phases at the high temperatures (900–1300 °C) necessary to obtain reasonable solid-state diffusion is often precluded because the phases are stable only at lower temperatures. Therefore, we are developing lower temperature synthesis strategies based on the reaction of suitable mixed-metal precursors with ammonia gas to produce ternary nitrides. Herein we report the synthesis of a new metallic, layered nitride, $LiMoN_2$, from two such precursors, and discuss its chemical and physical properties.

Experimental Section

Starting Materials. The precursor $Li_2Mo(N^tBu)_4$ was prepared according to published methods.[13] Lithium molybdate was prepared by heating a 1:1 mixture of Li_2CO_3 (99.99% metals purity) and MoO_3 (ACS grade) at 650 °C for approximately 18 h in air; Li_2MoO_4 was identified as a pure product by X-ray powder diffraction methods. All manipulations of $Li_2Mo(N^tBu)_4$ and $LiMoN_2$ were carried out in an argon-filled box or on a vacuum/argon manifold due to their known or anticipated air sensitivity.

Synthesis of $LiMoN_2$. The title compound was first synthesized by decomposing $Li_2Mo(N^tBu)_4$ (in an alumina boat) under flowing ammonia gas at 650 °C in a nitriding apparatus.[14] The product formed was a free-flowing, black powder that appeared graphitic on grinding. The X-ray powder pattern consisted of a small number of intense peaks and several weak peaks. The intense peaks could be indexed by assuming a hexagonal unit cell with a = 2.868 Å and c = 15.787 Å, with systematic zeroes that suggest rhombohedral symmetry. Since the weak peaks could not be indexed, the composition of the second phase is unknown. Since no binary Mo-N phases have these lattice parameters, it was clear that a ternary phase had formed. Due to the graphitic nature of the compound, we also suspected that the structure was layered.

Since $LiVS_2$ can be prepared by heating Li_2CO_3 and V_2O_5 in flowing H_2S gas at 750 °C,[15] it seemed possible that the a ternary nitride phase could be obtained by the reaction of Li_2MoO_4 with ammonia gas. We found that the same well-crystallized black powder, as identified by X-ray diffraction, could be prepared by exposing a melt of Li_2MoO_4 (in a 9.5 × 2 × 1 cm alumina boat) to flowing ammonia gas at 710 °C for 14 h in the nitriding apparatus. Again, weak peaks could be seen in the X-ray diffraction pattern. In this latter case, the weak peaks could be entirely accounted for by the presence of lithium oxide. The scale of the reaction is an important factor; when the mass of the Li_2MoO_4 is greater than about 1.5 g, incomplete reaction is observed. This may be due to slow kinetics once a thick nitride coat forms over the reactant. Grinding and re-reacting this powder lead to an increase in the anti-site defect concentration and partial decomposition (vide infra). The preparation of $Li_2Mo(N^tBu)_4$ is relatively time consuming, therefore we now exclusively synthesize the ternary nitride from Li_2MoO_4.

The thermal decomposition of Li_2MoO_4 in flowing ammonia gas occurs in at least a few distinct steps. When Li_2MoO_4 (solid) was heated in ammonia, it turned black at approximately 450 °C. Upon grinding, the powder was gray and the only crystalline phase detected by X-ray powder diffraction was Li_2MoO_4. This was indicative that a black, amorphous coat had formed on the Li_2MoO_4 particles. At 500 °C the powder was black when ground and one crystalline phase, Li_4MoO_5, was detected by X-ray diffraction. A second phase that must be present for mass balance remained amorphous. Within the range 650–710 °C, the ternary nitride and Li_2O were the only phases observed as determined by X-ray diffraction and mass loss from the reaction. Finally, by 850 °C the ternary nitride decomposed. All the lithium species sublimed, leaving only γ-Mo_2N in the reaction vessel as determined by X-ray diffraction and mass loss.

When a melt of Li_2MoO_4 (mp = 705 °C) was exposed to ammonia at 710 °C, a homogeneous, black powder quickly formed. Upon heating for 20 min at 710 °C and then quenching (at 710 °C), only Li_4MoO_5 was detected by X-ray diffraction. However, when the heating of this powder was continued for 12 h it was converted completely to the ternary phase and Li_2O.

The thermal stability of the ternary phase seems to lie in a fairly narrow temperature range. When reaction temperatures are below the melting point of Li_2MoO_4 (for example at 675 °C), the kinetics of the reaction are slowed dramatically yielding incomplete ammonolysis of the oxide. However, at temperatures greater than ~735 °C partial decomposition to γ-Mo_2N and a volatile lithium species is evident by X-ray powder diffraction and tube attack, as well as an increased concentration of anti-site defects in the ternary phase.

To determine the composition, structure, and properties of this new ternary nitride, it was necessary to remove the lithium oxide. Although the lithium oxide was readily removed by washing with water, the title compound appeared to be somewhat reactive toward water and/or aqueous base. Washing the nitride with water lead to a mass loss which was too great for the loss of lithium oxide exclusively; also some ammonia gas was produced as evident by its acrid odor. Washing with dried ethanol also removed the lithium oxide, but again it appeared to allow some small side reaction, as determined by new peaks in the X-ray diffraction pattern and mass loss, although the loss is much less than with water. We have not pursued this ethanol reaction further.

We found that the lithium oxide could be most successfully removed by condensing ammonia (approximately 10 mL of NH_3/0.15 g of nitride), predried over sodium, onto a mixture of ammonium chloride and the nitriding reaction product;[16] 2.2 mol of ammonium chloride was used for every mol of lithium oxide present. The products of this reaction are lithium chloride, ammonia, and water. This mixture was periodically stirred for 2 h at approximately −35 °C in an H-cell.[16] The ammonia was

(1) Gudat, A.; Rabenau, A.; Bronger, W.; Ruschewitz, U. *J. Less-Common. Met.* **1990**, *161*, 31.
(2) Gudat, A.; Haag, S.; Kniep, R.; Rabenau, A. *Z. Naturforsch.* **1990**, *45b*, 111.
(3) Juza, V. A.; Gieren, W.; Haug, J. Z. *Z. Anorg. Allg. Chem.* **1959**, *300*, 61.
(4) Chern, M. Y.; DiSalvo, F. J. *J. Solid State Chem.* **1990**, *88*, 459.
(5) Gudat, A.; Haag, S.; Kniep, R.; Rabenau, A. *J. Less-Common Met.* **1990**, *159*, L29.
(6) Chern, M. Y.; Vennos, D. A.; DiSalvo, F. J. *J. Solid State Chem.* **1992**, *96*, 415.
(7) Jacobs, H.; von Pinkowski, E. *J. Less-Common Met.* **1989**, *146*, 147.
(8) Vennos, D. A.; Badding, M. E.; DiSalvo, F. *J. Inorg. Chem.* **1990**, *29*, 4059.
(9) Cordier, G.; Hohn, P.; Kniep, R.; Rabenau, A. *Z. Anorg. Allg. Chem.*, in press.
(10) Gudat, A.; Hohn, P.; Kniep, R.; Rabenau, A. *Z. Naturforsch. B*, in press.
(11) Hohn, P.; Kniep, R.; Rabenau, A. *Z. Kristallogr.*, in press.
(12) Hohn, P.; et al. *Angew Chem., Int. Ed. Engl.* **1991**, *30*, 831.
(13) Danopoulos, A. A.; Wilkinson, G.; Hursthouse, M. B.; Hussain, B. *Polyhedron* **1989**, *8*, 2947.
(14) Rauch, P. E.; DiSalvo, F. J. *Inorg. Synth.*, in press.
(15) Murphy, D. W.; Cros, C.; DiSalvo, F. J.; Waszczak, J. V. *Inorg. Chem.* **1977**, *16*, 3027.
(16) Dye, J. L. Michigan State University, personal communication, 1991.

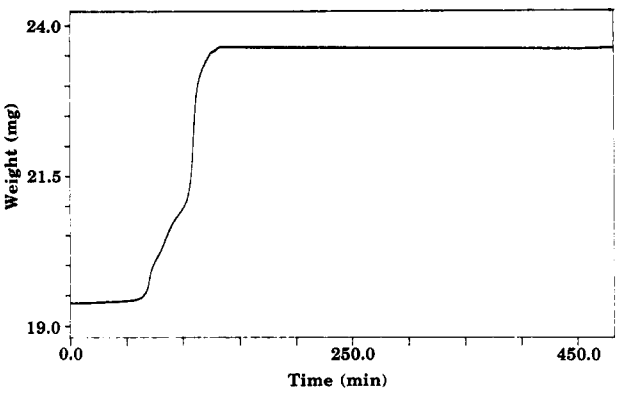

Figure 1. TGA of $LiMoN_2$ in air: 30 to 100 °C at 2 °C/min; 100 to 700 °C at 5 °C/min; 700 for 300 min; 700 to 30 °C at 25 °C/min.

decanted off, and the nitride was washed several times with fresh ammonia to remove the lithium chloride and any remaining ammonium chloride. The X-ray powder pattern was clean; no reactions with the ammonia or side products were evident. The presence of the small amount of water from this reaction did not seem to cause side reactions perhaps due to two factors: the reaction takes place below 0 °C leading to slow kinetics, and the small amount of water produced should be strongly coordinated to the lithium cations present.

Analysis. Solutions of the ternary phases were prepared by dissolution of the solids in aqua regia (this requires several hours at room temperature); Li_2MoO_4, dissolved in a like manner, was used as a standard. Metals analysis was done on solutions using plasma emission spectroscopy (PES). The molybdenum line (λ = 202.2 nm) was analyzed on a Jarrel-Ash I.C.A.P. 61 update spectrometer and the lithium line (λ = 670.8 nm) on a Model 82-000 modified Ebert Mount spectrometer. The Li:Mo ratio ranged from 0.95–0.97:1.00 leading to a stoichiometry (expected accuracy of ±2%) of $Li_{0.96}MoN_2$; we refer to this hereafter as $LiMoN_2$. Metals analysis (PES) indicated the stoichiometry (or the ratio of the metals) of the parent compound deintercalated (see section on chemical properties) with DDQ and $NOBF_4$ to be $Li_{0.44}MoN_2$ and $Li_{0.36}MoN_2$, respectively (assumed nitrogen content).

Since $LiMoN_2$ will not dissolve in H_3PO_4[17] or H_2SO_4 (Kjeldahl method), the nitrogen content could not be directly determined from evolved ammonia. Using the modified Dumas method,[18] we obtained 76% of the expected N_2. However, the sample could not be completely reacted with carbon dioxide even at 1000 °C as was evident by the black color of the sample after the reaction (complete reaction would leave a white oxide or carbonate powder). Consequently, this measurement can only put a lower limit on the N:Mo ratio of 1.5. However, by mass difference from the PES data, the N:Mo ratio is 2.2:1 (±15%).

The weight loss upon reaction of Li_2MoO_4 with ammonia was consistent with the formation of 0.5 mol of lithium oxide and 1 mol of $LiMoN_2$ for each mol of Li_2MoO_4. Also, the measured density[19] of $LiMoN_2$ powder was 5.72 g cm^{-3} (±2%) compared with the calculated density of 5.79 g cm^{-3} (see section on structure).

Although we have been unable to make a direct analysis for nitrogen, thermal gravimetric analysis (TGA) does give an upper limit of oxide contamination. Figure 1 shows the mass change upon heating $LiMoN_2$ in air. The TGA samples were exposed to the air for less than a minute during loading. Note that no degradation of $LiMoN_2$ is observed by X-ray powder diffraction or mass loss after several days of air exposure. The mass gain of 21.08% is close to the theoretical value of 21.38% for the decomposition of $LiMoN_2$ to $^1/_2Li_2O$ and MoO_3 or corresponding ternary oxides; this places an upper limit of about 10% oxygen content in the nitride (i.e., $LiMoN_{2-x}O_x$; $x < 0.2$). Coupled with the fact that the $LiMoN_2$ initially synthesized from $Li_2Mo(N^tBu)_4$ had lattice parameters identical to that of the $LiMoN_2$ prepared from the oxide, leads us to believe that the oxygen "contamination" is much smaller than 10%.

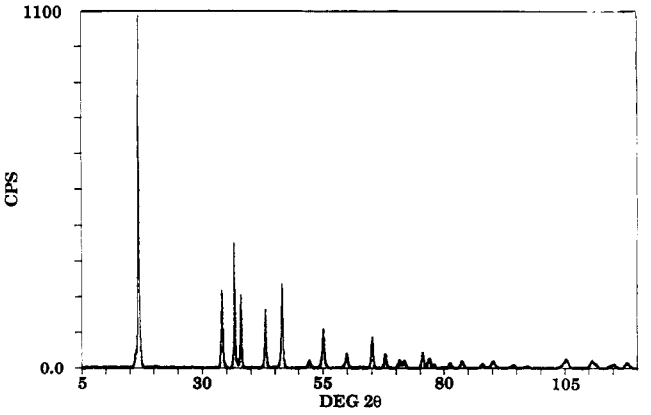

Figure 2. X-ray powder diffraction pattern of $LiMoN_2$.

Table I. Ideal Positional Parameters Initially Proposed for the Possible Structure of $LiMoN_2$

atom	site	x	y	z
	Space Group $R3$			
Mo	3a	0	0	0
Li	3a	0	0	5/6
N(1)	3a	0	0	1/4
N(2)	3a	0	0	5/12
	Space Group $R\bar{3}m$			
Mo	3a	0	0	0
Li	3b	0	0	1/2
N	6c	0	0	1/4

Table II. Calculated (00l) Intensities (Relative) for Different Anti-Site Defect Concentrations in $(Li_{1-x}Mo_y)_{oct}(Mo_{1-y}Li_x)_{tp}$ ($x = y$) Compared to Those Found Experimentally

x or y	003	006	009	0012	0015
0.0	100	11.3	4.7	3.5	1.1
0.15	100	22.6	4.6	6.8	1.3
0.25	100	43.2	4.5	13.0	1.4
exper	100	21.9	2.2	2.2	0.0

Structure Determination

X-ray Diffraction. Initial X-ray powder diffraction data[4] were collected with a Scintag XDS 2000 diffractometer (flat plate configuration) using Cu Kα radiation.

The X-ray powder pattern was easily indexed on a hexagonal unit cell with a = 2.868 Å and c = 15.787 Å. However, the systematic absences in the (10l) and the (00l) lines indicated that the correct space group is rhombohedral. Assuming that the structure consists of MoN_2 layers with close-packed layers of nitrogen sandwiching a layer of molybdenum and octahedral coordination for lithium (as is found in the layered sulfides), we were limited to two rhombohedral space groups: $R\bar{3}m$ (No. 166) and $R3$ (No. 146). The only difference between these two space groups is the nitrogen coordination about the molybdenum; $R\bar{3}m$ places the molybdenum in an octahedral hole while $R3$ places it in a trigonal prismatic one. Figure 2 shows the X-ray powder pattern and the assumed atomic positions in both space groups are listed in Table I.

By comparison of the experimental X-ray data to the calculated data,[20] we concluded that the molybdenum was in the trigonal prismatic hole. However, there are some significant differences between the measured and the calculated intensities. This is due in part to the preferred

(17) Bollman, D. H. *Anal. Chem.* **1972**, *44*, 887.
(18) Czechowicz, D. G., Los Alamos National Laboratory, personal communication, 1989.
(19) Chern, M. Y.; Mariani, R. D.; Vennos, D. A.; DiSalvo, F. J. *Rev. Sci. Instrum.* **1990**, *61*, 1733.
(20) Yvon, K.; Jeitschko, W.; Parthe, E. *J. Appl. Crystallogr.* **1977**, *10*, 73.

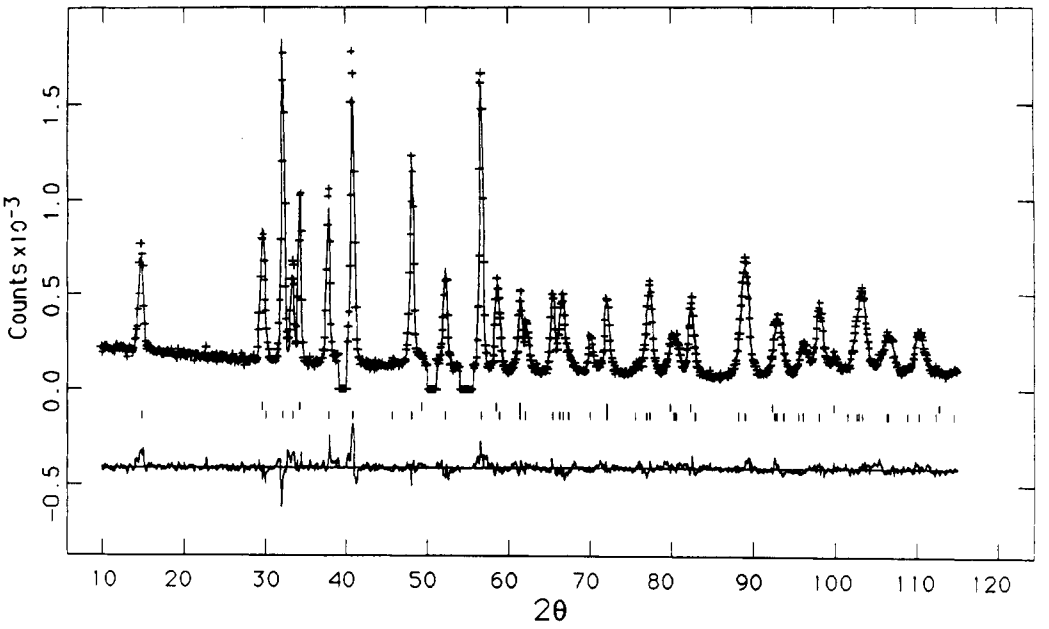

Figure 3. Neutron diffraction data for $LiMoN_2$ collected at 293 K at the steady-state source at Brookhaven National Lab (BNL). Points shown by + represent observed data. The continuous lines through the sets of points are the calculated profiles from refinements given in Table III. The tic marks below the data indicate the positions of the allowed reflections for both $LiMoN_2$ (bottom set) and Li_2O (top set). The lower curve represents the difference between observed and calculated profiles. Gaps in the pattern are regions containing peaks arising from impurities and were excluded from the refinement.

orientation that occurs when the graphite-like powder is packed into the X-ray sample holder which enhances out-of-plane reflections relative to the others. Even though the relative intensities of the (00*l*) reflections are not affected by preferred orientation, they show considerable variance with the calculated intensities for a model with purely trigonal prismatic molybdenum and purely octahedral lithium. This is especially evident in the relative intensities of the 003 and 006 lines. Since the stoichiometry and density are consistent with the ideal *R*3 structure, these X-ray data suggest anti-site defects may be present, as in Li_xCoO_2.[21] Table II shows how the calculated intensities in the (00*l*) series change for different concentrations of anti-site defects in the space group *R*3 along with what was found experimentally. The intensities of the 006, 009, 0012 and 0015 lines are less than those calculated for the different anti-site defect concentrations. These decreased intensities are likely due to line broadening from stacking faults, strain induced by the defects and increasing Debye–Waller factors at higher diffraction angles.

Calculated powder patterns which placed lithium in tetrahedral holes did not compare well with the experimental data and they led to structures that contained unreasonable lithium–nitrogen bond lengths (much shorter than the expected: Li–N ~ 2.0 Å).[22]

Since the X-ray intensity is proportional to Z^2 (Z = number of electrons), the detection of light atoms (i.e., lithium and nitrogen) in the presence of heavy ones is difficult. The scattering of neutrons is dependent only on the scattering length of a nucleus. This length may be as large for low-Z elements as it is for high-Z elements. Hence, neutron powder diffraction can be employed to obtain more detail about the structure.

In the case of $LiMoN_2$, the scattering length of N (b_N = 0.94) is larger than those for Mo (b_{Mo} = 0.69) and of Li (b_{Li} = −0.214). Consequently, neutron diffraction is likely to more accurately determine the nitrogen and lithium positions than X-ray diffraction, as well as aid in the determination of the defect concentration.

Neutron Diffraction. A 6-g sample of $LiMoN_2$ (a different sample than was used in the X-ray study) was loosely packed into a 1.5-cm-diameter vanadium can in an argon-filled drybox. An aluminum cap was secured to the top with epoxy to prevent air exposure. The Li_2O was not washed out because of the difficulty in handling such large volumes of liquid ammonia; hence this sample also contained about 0.5 g of Li_2O.

Neutron diffraction measurements on the sample were performed on a triple-axis diffractometer at the H4S station of the Brookhaven high flux beam reactor. The instrument configuration consisted of a pyrolytic graphite monochromator and analyzer, in the (002) and (004) settings, respectively, along with collimator of 20-ft in-pile, 40-ft monochromator sample, 40-ft sample analyzer and 20-ft analyzer-detector. The wavelength was calibrated using CeO_2 (a = 5.4113 Å), and its value was 1.3585 Å. The pattern, shown in Figure 3, was collected in 0.1° steps in 2θ from 5 to 130°. Inspection of the powder pattern data showed the presence of Li_2O as expected. Subsequent two phase refinement[23] suggested these components were in the molar ratio of 2:1, in agreement with the stoichiometry of the reaction

$$Li_2MoO_4 + \tfrac{7}{3}NH_3 \rightarrow LiMoN_2 + \tfrac{1}{2}Li_2O + \tfrac{1}{6}N_2 + \tfrac{7}{2}H_2O \quad (1)$$

In addition to the Li_2O peaks expected for the described synthetic procedure, some weak peaks, less than 1% of the strongest peak in the pattern, occurred near 33, 38, 52, and 56° 2θ. These were presumed to arise from an impurity phase (perhaps γ-Mo_2N), and these regions were excluded from the refinement.

A series of preliminary refinements indicated that molybdenum was in trigonal prismatic coordination with

(21) Thomas, M. G. S. R.; David, W. I. F.; Goodenough, J. B. *Mater. Res. Bull.* **1985**, *20*, 1137.
(22) Rabenau, A.; Schulz, H. *J. Less-Common Met.* **1976**, *50*, 155.
(23) Larson, A. C.; Von Dreele, R. B. *Generalized Structure Analysis System*; LANCE, MS-H805, Los Alamos National Laboratory, Los Alamos, NM 87545.

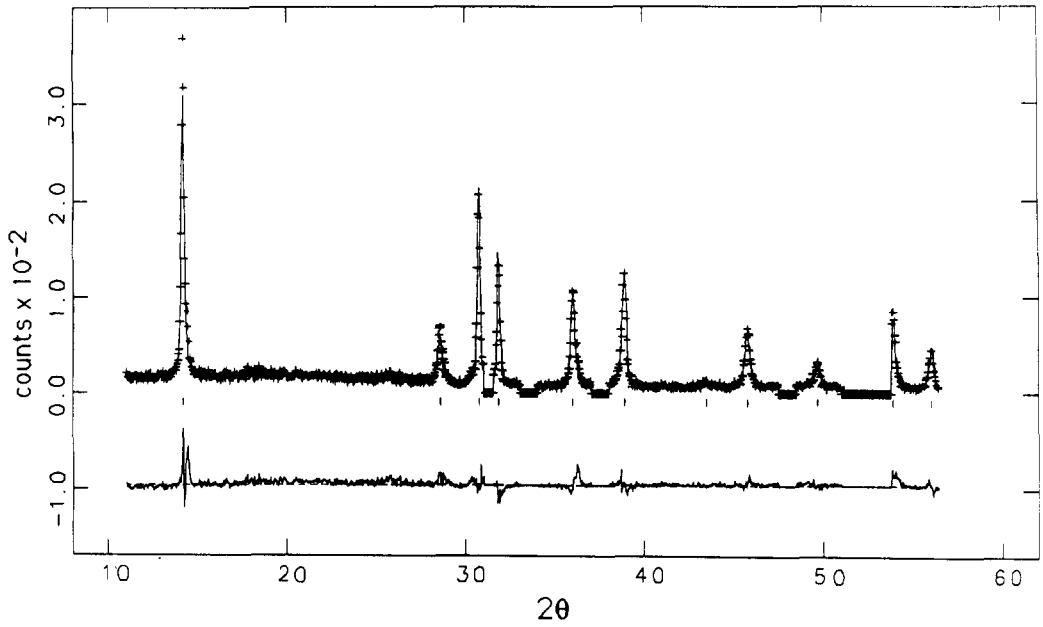

Figure 4. X-ray data for $LiMoN_2$ collected at 300 K at the National Synchrotron Light Source (NSLS) at BNL. Points shown as (+) represent observed data. The continuous lines through the sets of points are the calculated profiles from the refinements given in Table III. The set of tic marks below the data indicate the positions of the allowed reflections. Gaps in the pattern are regions containing peaks arising from impurities and were excluded from the refinement. The lower curve represents the difference between observed and calculated profiles.

nitrogen rather than octahedral, therefore further structure analysis was limited to space group $R3$. Locating the lithium proved to be problematic. No peaks could be discerned in the Fourier difference maps that were calculated on the basis of the partial structure model and intensities extracted from the neutron diffraction pattern.

A refinement of the occupancy factor for the molybdenum suggested the reason for the difficulty in locating the lithium site. Assuming the site to be occupied exclusively by molybdenum, its refined occupancy was 0.8 rather than 1.0. The stoichiometry $LiMoN_2$ is consistent with the chemistry of this material and the relative proportions of Li_2O and $LiMoN_2$ refined to 35% and 65% respectively, in agreement with eq 1. We assumed that there must be mixing between the lithium and molybdenum metal layers. As such, any deficiency in the molybdenum site should be coupled with a replacement of an equivalent of lithium in the lithium site by the molybdenum. The composition of the trigonal prismatic site can be easily estimated by (1) assuming the site to be fully occupied and (2) from the apparent scattering length observed for the site, presuming it to contain only molybdenum. Simultaneous solution of the equations suggested a trigonal prismatic composition of $(Mo_{0.85}Li_{0.15})$ which implies $(Li_{0.85}Mo_{0.15})$ to be located at the yet-undisclosed lithium site. The total scattering expected from the latter site is then $(0.85b_{Li} + 0.15b_{Mo} = -0.08)$, where the b's refer to the scattering lengths of the elements occupying this site at random within the structure. Hence, the scattering of neutrons from the lithium rich site is about zero, which is consistent with the lack of peaks in the Fourier difference map.

To determine the molybdenum occupancy and position on the lithium-rich site, X-ray diffraction data must be included in the refinement. At $\sin\theta/\lambda = 0.0$ the scattering expected for each lithium rich site is about $0.85f_{Li} + 0.15f_{Mo} = 8.9$ electrons.

Synchrotron X-ray Diffraction. X-ray diffraction intensity measurements were performed at the X-7A beamline at the National Synchrotron Light Source (NSLS). A channel cut Si(111) monochromator and a Ge(220) analyzer were used,[24] and the wavelength was determined to be 1.29812 Å from a CeO_2 standard. Data were collected (Figure 4) in the range 10–56° 2θ with a step size of 0.01° in 2θ with a counting time of 5 s/step. The instrument was configured in the high-resolution mode using a Kevex detector (this utilizes Debye–Scherrer diffraction geometry which corrects for the preferred orientation expected in this layered material).[24] Beam defining slits of 0.65 × 12 mm were used. Corrections were made for detector dead-time and absorption. The value of μR was estimated to be 1.30 for the sample, which was contained in a glass capillary with a diameter of 0.5 mm (μ is the absorption coefficient and R is the radius of the capillary). A packing density of 30% was assumed.[24]

Using the parameters obtained for the structure model derived from the neutron data, a Fourier difference map was calculated based on the X-ray data. This revealed a peak of height 5 electrons/Å^{-3} in the octahedral site between the MoN_2 layers. This was estimated to correspond to 0.12 Mo. Inclusion of this site lowered the weighted profile discrepancy from 0.297 to 0.260. Inclusion of this same amount of scattering at the tetrahedral site $(0,0,^1/_2)$ raised the discrepancy to 0.341.

The unique information offered by the X-ray and neutron experiments were combined in a refinement using both the X-ray and neutron powder diffraction data. Since these two sets of data were collected at different temperatures, they were treated as two different $LiMoN_2$ phases. The difference in the temperatures at which the two data sets were collected was small, 7 K, but this caused a measurable difference in the c cell parameter (see Table III). The position and thermal parameters for the two phases were constrained to be equal. The third phase defined was Li_2O, a significant component of the sample used in the data collection. Both data sets were corrected for the effects of absorption.[24]

The model was refined with lithium and molybdenum mixed in the trigonal prismatic site and the inter-layer octahedral site. The refinement was constrained such that

(24) Cox, D. E.; Toby, B. H.; Eddy, M. M. *Aust. J. Phys.* **1988**, *41*, 117.

Table III. Refined Positional and Thermal Parameters from the Joint X-ray[a] and Neutron[b] Refinement of $LiMoN_2$ ($R3$, $Z = 3$)[c]

atom	site	x	y	z	U_{iso} (Å² × 100)
Mo(1)[d]	3a	0.0	0.0	0.0	0.6 (1)
Li(1)[d]	3a	0.0	0.0	0.8290 (18)	5.7 (8)
N(1)	3a	0.0	0.0	0.2520 (4)	2.5 (1)
N(2)	3a	0.0	0.0	0.4141 (4)	1.6 (1)

[a] Refined cell parameters (Å) for the X-ray case: a = 2.8672 (3), c = 15.813 (3); R_{wp} = 0.185, R_p = 0.144, R_N = 0.057. The peak shape for the synchrotron X-ray data was fit with Lorentzian and Gaussian functions. U = 1950, V = −1648, and W = 572 were the profile coefficients for the Gaussian portion. X = 8.9, Y = 26, and Z = 7.2 were the profile coefficients for the Lorentzian portion. The asymmetric parameter A_s (in the (00l) direction) = 10.4.[23] [b] Refined cell parameters (Å) for the neutron case: a = 2.8674 (2), c = 15.801 (2); R_{wp} = 0.093, R_p = 0.074, R_N = 0.057. The background for the neutron data was fit using a cosine Fourier series; the peak shape was modeled with a Gaussian function modified for peak asymmetry with A_s = 8.8, U = 2427, V = −1794, and W = 600. The anisotropic peak broadening coefficient (in (00l) direction) = 53.[23] [c] Overall powder statistics for both refinements: R_{wp} = 0.128, R_p = 0.079, χ^2 = 2.01. [d] Partially occupied sites: the site designated Mo(1) has composition ($Mo_{0.850(5)}Li_{0.150(5)}$) and the Li(1) site has the constrained composition ($Mo_{0.150(5)}Li_{0.850(5)}$), thereby ensuring the overall stoichiometry for the phase $LiMoN_2$.

Table IV. Selected Interatomic Distances (Å) and Angles (deg) for $LiMoN_2$

Bond Distances			
Mo(1)–N(1) × 3	2.095 (4)	Li(1)–N(1) × 3	2.179 (18)
Mo(1)–N(2) × 3	2.091 (4)	Li(1)–N(2) × 3	2.098 (17)
Angles			
N(1)–Mo(1)–N(1) × 6	86.34 (9)	N(1)–Li(1)–N(2) × 6	95.72 (8)
N(1)–Mo(1)–N(2) × 3	75.45 (9)	N(1)–Li(1)–N(2) × 3	177.3 (9)
N(1)–Mo(1)–N(2) × 6	133.41 (3)	N(2)–Li(1)–N(2) × 3	86.2 (9)
N(1)–Li(1)–N(1) × 3	82.3 (8)		

the formula $LiMoN_2$ was maintained, and all sites were presumed to be fully occupied {i.e., $(Li_{1-x}Mo_y)_{oct}$-$(Mo_{1-y}Li_x)_{tp}N_2$, where $x = y$}. The z parameter of the molybdenum site in both phases was fixed at zero in order to define the origin along the c axis.

The thermal parameters for the lithium site were comparatively large and may indicate some positional disorder for the lithium and molybdenum. The resulting structure and structural data from the refinement are displayed in Figure 5 and Tables III and IV.

It is interesting to note that when the refinement was carried out using only the neutron data, the z parameter of the lithium-rich site varied considerably. The nitrogen z parameters behaved in a similar way when only the X-ray data was refined. This is a direct consequence of the net near-zero scattering length and the low scattering power of nitrogen, respectively. It is evident why both data sets were necessary in the final refinement and why the positional and thermal parameters were constrained to be equal for the corresponding atoms in each data set.

We have observed in X-ray powder diffraction experiments that when $LiMoN_2$ is reheated in ammonia gas, the 006 line intensity increases by as much as 15%, indicating that the anti-site defect concentration or the disorder is increasing. We also considered the possibility that the structure may at least partially order at a low temperature. A sample of $LiMoN_2$, containing 15% anti-site defects, was sealed in an evacuated quartz tube and annealed at 300 °C for 34 days. An X-ray pattern of the resulting black powder showed no visible decomposition and the relative intensities of the 003 and 006 reflections remained the same, indicating that the anti-site defect concentration was unaffected.

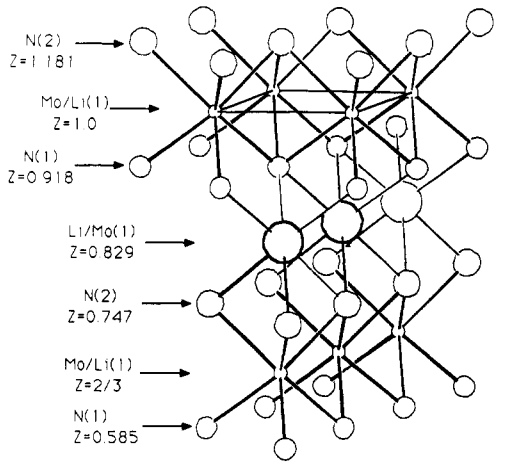

Figure 5. Part of the structure of $LiMoN_2$ emphasizing the coordination of the site between the MoN_2 layers that is predominantly occupied by Li (large circles). The (001) face of the unit cell is outlined.

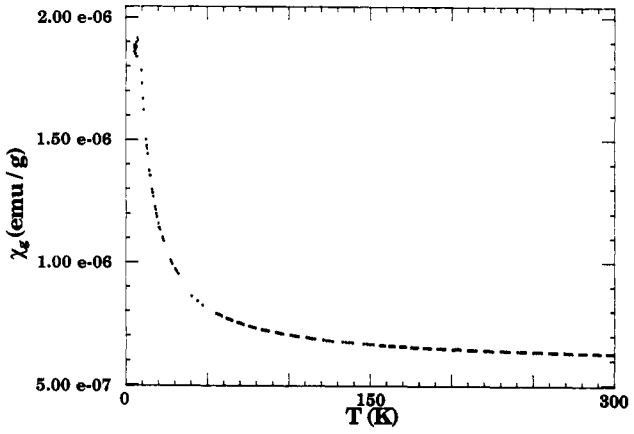

Figure 6. Temperature-dependent susceptibility of $LiMoN_2$.

Magnetic Susceptibility. The magnetic susceptibility was measured from 4.2 to 300 K on a previously calibrated[25] Faraday balance; the sample was sealed in a thin-walled Suprasil quartz tube under a partial pressure of helium. The room-temperature susceptibility exhibited some magnetic field dependence indicative of a small amount of ferromagnetic impurity. The signal from the ferromagnetic impurity was subtracted by the method of Owen and Honda[26] and the corrected data are shown in Figure 6. The Curie tail at low temperature (the increase in χ as T is lowered) can be attributed to a small amount of paramagnetic impurity. We fit the data to $\chi_g = \chi_0 + C_g/(T + \theta)$ by a least-squares method over the temperature range 4.2–300 K. We obtained $C_g = 1.15 \times 10^{-5}$ emu g^{-1}, $\theta = 0$, and $\chi_0 = 0.59 \times 10^{-6}$ emu g^{-1} (±2%) with a mean-square deviation of data to the fit of 0.6%. This value of χ_0 is in the range of observed values for transition metals.[27] The magnitude of C_g is consistent with ~0.04 at. % iron (assuming $g = 2$, $S = 2$) impurity concentration. Although we have not directly measured impurity levels, iron is the most common paramagnetic impurity in solids and the calculated impurity level is consistent with the purity of the starting materials.

Electrical Properties. A simple two-point resistance measurement of $LiMoN_2$ was made by pressing a sample

(25) Vassiliou, J.; Hornbostel, M.; Ziebarth, R.; DiSalvo, F. J. *J. Solid State Chem.* **1989**, *81*, 208.
(26) Selwood, P. W. *Magnetochemistry*; Wiley-Interscience: New York, 1979; p 186.
(27) Kriessman, C. J. *Rev. Mod. Phys.* **1953**, *25*, 122.

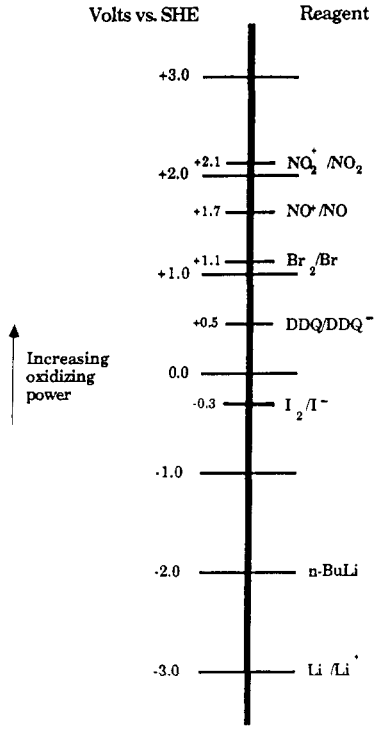

Figure 7. Approximate potentials (vs standard hydrogen electrode) of the oxidizing agents, in dry acetonitrile, used for the deintercalation of $LiMoN_2$ (adapted from ref 27).

of the powder (2.3-mm thickness, 2.6-mm diameter) between two metal rods in an insulating alumina cylinder. The resistance of the pellet was less than 0.01 Ω (the lower limit of the measurement) greater than that measured when no powder was present between the rods; this led to a calculated resistivity at room temperature of less than or equal to 2×10^{-3} Ω cm. One major limitation of the two probe method is that it may be dominated by particle–particle contact resistance. Consequently, we can presently give only an upper limit of resistivity. Attempts to make sintered pellets for four-probe resistivity measurements were unsuccessful due to the fragile nature of the pressed pellets.

Chemical Properties. Lithium can generally be intercalated into or deintercalated from layered structures; hence we attempted such reactions with $LiMoN_2$.

Several oxidizing agents to remove lithium from $LiMoN_2$ were investigated, including I_2, Br_2, DDQ (2,3-dichloro-5,6-dicyanobenzoquinone), $NOBF_4$, and NO_2BF_4. The potentials of these oxidizing agents (in acetonitrile) versus a standard hydrogen electrode are shown in Figure 7.[28] The expected reactions, if all lithium were removed, are, for example, given in eqs 2–6. In each case the product salts are soluble in acetonitrile, while the MoN_2 and $LiMoN_2$ are insoluble.

$$LiMoN_2 + \tfrac{1}{2}I_2 \rightarrow MoN_2 + LiI \quad (2)$$

$$LiMoN_2 + \tfrac{1}{2}Br_2 \rightarrow MoN_2 + LiBr \quad (3)$$

$$LiMoN_2 + DDQ \rightarrow MoN_2 + Li^+DDQ^- \quad (4)$$

$$LiMoN_2 + NOBF_4 \rightarrow MoN_2 + LiBF_4 + NO(g) \quad (5)$$

$$LiMoN_2 + NO_2BF_4 \rightarrow MoN_2 + LiBF_4 + NO_2(g) \quad (6)$$

The general procedure was to reflux approximately 150 mg of the nitride with a 2-fold excess of the oxidizing agent dissolved in 50 mL of dry (stirred over powdered 3-Å sieves for at least 24 h) acetonitrile for 1–2 days. The mixture was filtered, washed with fresh acetonitrile, and dried in the globebox under vacuum. The extent of both deintercalation and side reaction was determined by X-ray powder diffraction, mass loss, and PES analysis (see section on analysis).

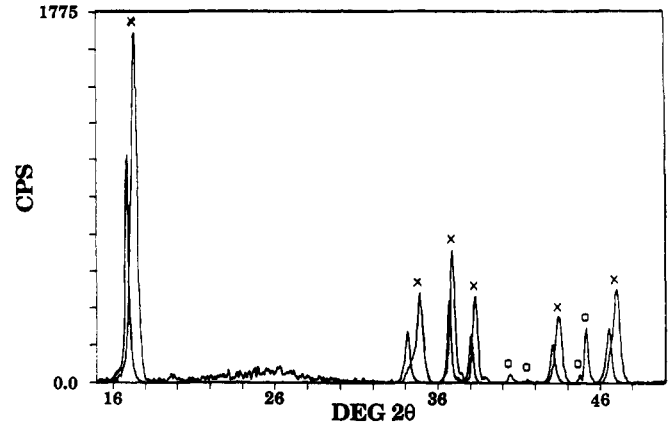

Figure 8. X-ray powder pattern of $Li_{0.36}MoN_2$ (deintercalated with $NOBF_4$) superimposed on the powder pattern for $LiMoN_2$. $Li_{0.36}MoN_2$ peaks are denoted by an × and second phase peaks (introduced by the deintercalation reaction) by an O.

No decolorization of the iodine (0.1 M in acetonitrile) solution was observed when 1 equiv of iodine was refluxed with the nitride. Furthermore, there was little or no lithium iodide formation (no mass change of the black $LiMoN_2$ powder), and there were no changes in the X-ray powder diffraction pattern. We concluded that iodine was not a strong enough oxidizing agent.

The oxidizing power of the remaining agents was strong enough for at least partial deintercalation. When the first 0.1–0.2 equiv of bromine solution (0.1 M in acetonitrile) was added, decolorization of the solution was observed indicating deintercalation. However, when more than 0.2 equiv of bromine was added, the solution became yellow, indicating some decomposition of the $LiMoN_2$. The resulting X-ray powder pattern showed some broadening of the peaks, indicating that a small fraction of lithium had indeed been removed.

In the case of $NOBF_4$ and NO_2BF_4 the evolution of gas (NO and NO_2) was observed, which was indicative of reaction. However, there was a reasonable amount of decomposition of the nitride with the use of $NOBF_4$ and NO_2BF_4. This was indicated by a yellow or brown filtrate after refluxing and washing the nitride and by a mass loss greater than expected for the removal of 1 equiv of lithium from $LiMoN_2$. The products of decomposition have not been studied. The reflections in the X-ray powder diffraction pattern shift upon removal of lithium; most noticeably the (00*l*) series, as expected for a layered structure. The X-ray powder pattern of the most lithium deficient phase obtained, $Li_{0.36}MoN_2$, is compared to that for $LiMoN_2$ in Figure 8. The lattice constants for $Li_{0.36}MoN_2$ were $a = 2.862$ Å and $c = 15.529$ Å. Several small peaks, indicative of the presence of a second phase, appear when the average lithium content is below ~0.5 Li/Mo. These phases have yet to be studied. Table V compares the *d* spacings observed in both $LiMoN_2$ and $Li_{0.36}MoN_2$.

The evolved NO(g) and NO_2(g) also appear to react with the nitride. When the gases were swept away by bubbling argon gas through the solution at ~0.5 cm^3/s, the deintercalated nitride could be reintercalated with *n*-butyllithium (in hexane) at room temperature as was indicated by a shift of the lines in the X-ray diffraction pattern back

(28) Wizansky, A. R.; Rauch, P. E.; DiSalvo, F. J. *J. Solid State Chem.* 1989, *81*, 208.

Table V. Observed d Spacings for $LiMoN_2$ and $LiMoN_2$ Deintercalated with $NOBF_4$ As Determined by X-ray Powder Diffraction

	d, Å	
$h\ k\ l$	$LiMoN_2$	Li_xMoN_2 (x = 0.36)
0 0 3	5.250	5.167
0 0 6	2.631	2.586
1 0 1	2.452	2.448
1 0 2	2.368	2.361
		2.239[a]
		2.185[a]
1 0 4	2.101	2.090
		2.032[a]
		2.015[a]
1 0 5	1.952	1.939

[a] Refers to second-phase peaks.

to the original positions observed in $LiMoN_2$. If the evolved gas was not rapidly removed during the refluxing process, the resulting deintercalated species could not be reintercalated with *n*-butyllithium. It was likely that a pacifying coating had formed on the particles due to these oxidizing gases.

Reaction with DDQ produced a deep reddish orange solution which was consistent with the formation of the Li^+DDQ^- salt. The mass loss was consistent with little or no side reaction. When DDQ was the oxidizing agent, the d spacings for the (00l) lines of the product were shifted to positions intermediate of those for $LiMoN_2$ and $Li_{0.36}MoN_2$ (see section on analysis).

While we have succeeded in deintercalating $LiMoN_2$ chemically, none of the oxidizing agents could remove all the lithium.

Electrochemistry. To better understand the behavior of $LiMoN_2$ with respect to lithium intercalation, we performed electrochemical measurements using Swagelock test cells assembled in a helium-filled drybox.[29] The positive electrode was a pressed pellet which consisted of 10 mg $LiMoN_2$, 9% carbon black, and 1% EPDM (ethylenepropylenediene monomer, used as a binder); the negative electrode was a lithium disk. The electrodes were separated by a porous glass filter paper soaked in an electrolyte that consisted of a 1 M solution of $LiClO_4$ in a 50–50 ethylene carbonate (EC)–diethoxyethane (DEE) mixture. The electrochemical cells were studied in both galvanostatic and potentiostatic modes using a Mac Pile system.[30] By monitoring the voltage of a $LiMoN_2$/Li cell while it was charged and discharged at constant current (galvanostatic mode), we observed a large voltage polarization (voltage difference between open-circuit and closed circuit curves) suggesting that the kinetics of the lithium deintercalation process in $LiMoN_2$ is very slow. Because of this early finding, we have mainly used the potentiostatic mode to further study this system.

The voltage–composition curves are shown for two electrochemical cells in Figures 9 and 10. Cell 1 (Figure 9) has been charged at a scan rate of 2 mV/h up to 4.2 V and then discharged to 2.7 V, while cell 2 (Figure 10) has been charged to 4.1 V at a higher scan rate of 10 mV/h and then cycled once between 4.1 and 0.02 V.

In cell 1, we note on charging the presence of two pseudoplateaus located at an average voltage of 3.73 and 4.07 V, corresponding to a capacity of about 100 and 75 mA h/g respectively. On the discharge following the second plateau, an oxidative capacity is still observed,

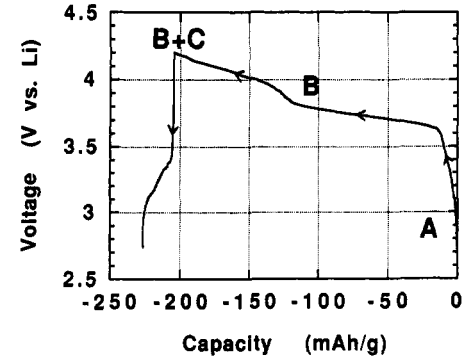

Figure 9. Voltage–composition curve for cell 1. It was charged to 4.2 V at 2 mV/h and then discharged to 2.7 V. Phase A is $LiMoN_2$, phase B is a lithium-poor phase ($Li_{1-x}MoN_2$), and phase C results from the oxidative decomposition of B.

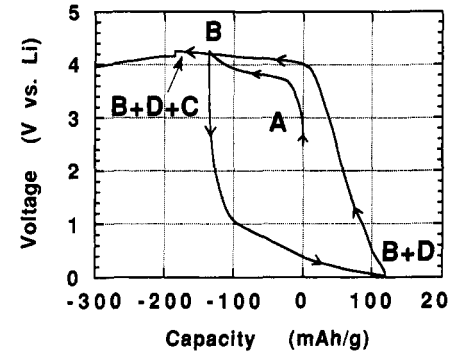

Figure 10. Voltage–composition curve for cell 2. It was charged to 4.1 V at 10 mV/h and then cycled between 4.1 and 0.02 V for one cycle. Phases A–C are the same as in Figure 9; phase D results from the reductive decomposition of B.

indicating unambiguously a decomposition reaction either of the electrolyte or of the electrode material. Since the electrolyte has been found stable to 4.5 V in separate experiments, we conclude that the pseudoplateau observed at 4.07 V is due to the oxidative degradation of the $LiMoN_2$ electrode material. This is consistent with the blue color of the electrolyte that is observed upon opening the cell, indicative of the presence of Mo^{x+} species in solution.

To determine the origin of the pseudoplateau at 3.73V, cell 2 was charged at a higher scan rate than cell 1, but to a lower charging cutoff voltage (4.1 V) in order to prevent the decomposition reaction. A single pseudoplateau located at an average of 3.8 V and corresponding to a 110 mA h/g capacity is observed. This plateau is identical to that observed for cell 1 at 3.73 V. The higher voltage observed for the higher scan rate used to cycle the cell is a further indication of the very slow electrochemical process. The plateau corresponds to the deintercalation of lithium from the layered structure as suggested by the X-ray powder pattern recorded at the end of the charge. On discharge, the voltage of the cell drops sharply to 1.5 V and then smoothly to 0.02 V so that a capacity of 255 mA h/g is measured. Because the "reduction" reaction occurs at an average voltage of 0.4 V (far from the voltage of the deintercalation reaction), it is unlikely that this capacity is due to the insertion of lithium into the structure. At this very low voltage, a likely possibility could be the reductive degradation of the material. This is consistent with the observation that on the second charge, after being discharged to 0.02 V, the voltage–composition curve of the cell does not trace back the first charge but is shifted to a higher voltage so that there is a pseudoplateau located at 4.05 V instead of 3.8 V as in the first charge. However, the nature of the pseudoplateau at 4.05

(29) Guyomard, D.; Tarascon, J. M. *J. Electrochem. Soc.*, in press.
(30) Mac Pile Data Acquisition System for Insertion Compounds, CNRS, Grenoble, France.

V is quite different from that at 3.8 V, which corresponds to lithium deintercalation, but rather similar to the the decomposition plateau observed for cell 1 at 4.05 V. When this cell is maintained at a charge of 4.05 V, an oxidative capacity is still observed on discharge which is characteristic of the decomposition of the electrode material.

A possible scenario to describe the behavior of the $LiMoN_2$/Li cell is that upon charging to 4.1 V, the starting $LiMoN_2$ phase (denoted A) is transformed to a lithium-poor phase (B). Upon further charging, the B phase decomposes to a C phase. Therefore, for voltages greater than 4.1 V our electrode consists of a mixture of the phases B and C. The discharge of the cell from 4.1 V results in another phase (D). When the cell reached 0.02 V, the electrode is a mixture of the B and D phases (it takes at least five electrons to reduce the B phase completely); upon recharge the cell potential reaches a plateau at 4.1 V that again corresponds to a decomposition of the B phase into the C phase.

Discussion

The ideal structure of $LiMoN_2$ is composed of stacked hexagonal close-packed sheets of nitrogen with the molybdenum in trigonal prismatic coordination between nitrogen sheets and lithium in octahedral coordination. The X-ray/neutron diffraction data unequivocally show that the molybdenum is in trigonal prismatic coordination in the predominantly molybdenum layers as predicted for d^1 transition metals in layered dichalcogenide compounds,[31] and the lithium is in octahedral coordination in the predominantly lithium layers. However, the data indicate that there are on the order of 15% anti-site defects in the lithium and molybdenum metal layers. The defect concentration appears to be unchanged when $LiMoN_2$ is annealed at 300 °C.

The Mo–Mo distance of 2.8674 Å (from the neutron refinement) is close to that found in molybdenum metal (2.73 Å), but there were no superlattice reflections observed in either the X-ray or neutron data, ruling out the possibility of molybdenum clusters.[32,33]

The N–N distance between the opposing nitrogen sheets in the MoN_2 layer is 2.56 Å, while the in-plane distance is 2.87 Å and the interlayer N–N distance is 3.17 Å. The former distance (2.56 Å) is the shortest reported for any binary or ternary nitride; for example, TiN (3.00 Å),[34] Ta_3N_5 (2.63 Å),[35] or Ca_3CrN_3 (3.01 Å). The data suggest that the N–N distance decreases as the covalency of the metal–nitrogen bonding increases. Although this intralayer nitrogen separation is much longer than 1.47 Å found for the N–N single bond in hydrazine,[36] calculations have shown that there is a small N–N interaction between closest nitrogens in the MoN_2 layer.[37]

The molybdenum of $LiMoN_2$ has a formal oxidation state of +5; this d^1 electron configuration is expected independent of the covalency of the Mo–N bond. However, to the extent that N–N bonding exists, the molybdenum electron configuration would be increased to $d^{1+\delta}$. Since the N–N bonding is assumed to be small from bond length comparisons, we assume δ is also small. Nevertheless, it is reasonable to predict that this compound should exhibit metallic behavior as in for example 2*H*-TaS_2 or 2*H*-$NbSe_2$.[31] We have found supporting evidence for this: black in color, Pauli-paramagnetic behavior, and a resistivity less than 2×10^{-3} Ω cm.

In contrast to $LiMoN_2$, $LiMoO_2$ crystallizes in two different structures. The low-temperature form,[38] which is prepared by intercalating lithium into MoO_2 at room temperature, has a distorted rutile structure and crystallizes in the space group $P2_1/c$. The high-temperature form, prepared by reacting Li_2MoO_4 with molybdenum metal at 900 °C, has a hexagonal layered structure ($R\bar{3}m$).[39] In both structural forms, the molybdenum (d^3) and lithium atoms are in octahedral holes.

The asymmetric peaks (Figure 8) of the deintercalated $LiMoN_2$ are likely due to inhomogeneous removal of the lithium: some particles contain more lithium than others or the region near particle surfaces contains less lithium than the middle of the particles. It seems reasonable that this could be quite sensitive to the particle size distribution and to the actual diffusion rate, or the possibility that $Li_{1-x}MoN_2$ may not form a continuous single phase for all x.

None of the chemical oxidizing agents were able to completely deintercalate the lithium. This may be due in part to a lower lithium diffusion rate at low lithium content, the 0.15Li in the molybdenum layer may be much less mobile than the lithium in the the lithium-rich layer or the potential needed to remove more and more lithium exceeds the oxidizing power of the deintercalating agents being used. This latter possibility is supported by the analytical data showing that more lithium can be deintercalated by $NOBF_4$ (+4.7 V vs Li/Li^+) than by DDQ (+4.1 V vs Li/Li^+). Unfortunately, good PES data were not consistently obtained for the deintercalation products that resulted from using NO_2BF_4 (+5.1 V vs Li/Li^+). The lithium can be reinserted at room temperature with *n*-butyllithium if the oxidizing gases (NO and NO_2) are swept away.

From the electrochemical data, one can conclude that 0.6Li can be removed from the structure by charging the cell to 4.1 V which is in reasonable agreement with the chemical deintercalation data. Attempts to remove more than 0.6Li resulted in an oxidative decomposition of the $LiMoN_2$ phase. This electrochemical process is not reversible since attempts to reinsert lithium electrochemically have been unsuccessful. It is unusual that reintercalation cannot be accomplished electrochemically while chemically it can be. If it is assumed that some oxidative degradation occurs in both methods of deintercalation, it is possible that the degradation product is soluble in refluxing acetonitrile, effectively cleaning the particle surfaces and making reintercalation possible. However, in the electrochemical case the particles may remain coated, making it difficult for reintercalation, thus requiring lower potentials for insertion and eventually reductive degradation.

The electrochemical properties of a compound are usually directly related to their structure. The neutron diffraction data indicate the presence of anti-site defects, and it is well-known that the presence of 3d metal ions within the lithium layers slows the kinetics of the intercalation/deintercalation chemistry considerably.[21] It is pos-

(31) Mattheiss, L. F. *Phys. Rev. B.* **1973**, *8*, 3719.
(32) Goodenough, J. B. Presented at the 4th Chem. Uses Molybdenum, Proc. Int. Conf, Ann Arbor, MI, 1982.
(33) Corbett, J. D.; McCarley, R. E. In *Crystal Chemistry and Properties of Materials with Quasi-One-Dimensional Structures*; Rouxel, J., Ed.; Reidel: Dordrecht, Netherlands, 1986; p 179.
(34) Beattie, H. J.; VerSnyder, F. L. *Trans. Am. Soc. Met.* **1953**, *45*, 397.
(35) Brese, N.; O'Keefe, M.; Rauch, P. E.; DiSalvo, F. J. *Acta Crystallogr.* **1991**, *C47*, 2291.
(36) Jolly, W. L. *The Inorganic Chemistry of Nitrogen*; W. A. Benjamin, Inc.: New York, 1964; p 58.
(37) Singh, D. J., Naval Research Labs, personal communication, 1992.
(38) Murphy, D. W.; DiSalvo, F. J.; Carides, J. N.; Waszczak, J. V. *Mater. Res. Bull.* **1978**, *13*, 1395.
(39) Aleandri, L. E.; McCarley, R. E. *Inorg. Chem.* **1988**, *27*, 1041.

sible that as lithium is being removed from the structure the anti-site defect concentration is increased, blocking the lithium diffusion paths and making subsequent lithium intercalation/deintercalation more difficult or even impossible.[40,41] This may also be a source of irreversibility in the electrochemical reactions.

Conclusion

We have discovered the first metallic, layered lithium ternary nitride, $LiMoN_2$. This is the first reported synthesis of a ternary nitride from molecular ($Li_2Mo(N^tBu)_4$) or oxide (Li_2MoO_4) precursors. The structure has cation anti-site defects at the level of 15%. Up to 64% of the lithium can be chemically deintercalated and reintercalated. However, in electrochemical cells little reversibility is seen. The high degree of covalency in this material produces the shortest N-N contacts of any known nitride, and may result in a weak N-N interaction. Recent electronic structure calculations on the *hypothetical ordered structure* indicate a signifiant amount of nitrogen contribution to the wave functions at the Fermi level.[37] This has prompted us to search for alternative synthetic conditions and routes to achieve this ordered state.

The chemistry and properties of the lithium intercalated dichalcogenide layered compounds $LiMX_2$ (X = S, Se; M = IVb, Vb, VIb transition metals)[42,43] and the layered oxides[21] have been known and studied for over 25 years. Long term interest in these materials is due in part to their potential use in recyclable lithium batteries[44] and as catalysts. The discovery of $LiMoN_2$ affords a rare opportunity to compare the structure and properties of a material intermediate to the analogous layered ternary chalcogenides and oxides. The structure is similar to that found in the chalcogenides and oxides, and in general the physical and chemical properties can be rationalized on the basis of the models developed for those materials. The major difference is in the degree of covalency in the metal-nitrogen bonding, being less than in chalcogenides and more than in the oxides, which does have subtle affects on the physical and electronic structure.[37]

Acknowledgment. We are grateful to the Office of Naval Research for its generous support of our nitride work and the Department of Education Fellowship supporting S.H.E. We are are also grateful to Mike Rutzke in the Department of Fruit and Vegetables at Cornell University for assistance in the PES analysis, Daccai Xie at the H4S high flux beam reactor at BNL for collecting the neutron diffraction data and Joe Hriljac for the synchrotron X-ray diffraction data collection on beamline X-7A at NSLS supported by the Division of Materials Science (DOE) under contract DE-AC02-76CH0001 to D. E. Cox.

(40) Murphy, D. W. *NATO Conf. Ser. E* **1985**, *101*, 181.
(41) Sandre, E.; Brec, R.; Rouxel, J. *J. Solid State Chem.* **1990**, *88*, 269.
(42) Whittingham, M. S. *Prog. Solid State Chem.* **1978**, *12*, 41.
(43) Rouxel, J. *In Physics and Chemistry of Compounds with Layered Structures*; Levy F., Ed.; Reidel: Dordrecht, Netherlands, 1979; p 201.
(44) Whittingham, M. S. *J. Electrochem. Soc.* **1976**, *123*, 315.

Ammonia-Induced Pyrolytic Conversion of a Vinylic Polysilane to Silicon Nitride

Wayde R. Schmidt,*,† Paul S. Marchetti,‡ Leonard V. Interrante,*,§ William J. Hurley, Jr.,† Russell H. Lewis,‡ Robert H. Doremus,† and Gary E. Maciel‡

Department of Materials Engineering, Rensselaer Polytechnic Institute, Troy, New York, 12180-3590; Department of Chemistry, Colorado State University, Fort Collins, Colorado 80523; and Department of Chemistry, Rensselaer Polytechnic Institute, Troy, New York, 12180-3590

Received April 9, 1992. Revised Manuscript Received June 5, 1992

The decomposition of a vinylic polysilane precursor to Si_3N_4 was examined during thermolysis of the polymer from 25 to 1000 °C in anhydrous NH_3. The polymer cross-links primarily through pendant vinyl groups below 300 °C in NH_3 into a rigid, highly porous solid. Ammonia provides the source of N, which is incorporated into the originally N-free polysilane, and acts to quench free radicals which are formed during decomposition of the polymer. Significant incorporation of N into the polymer, with associated loss of C, occurs between 300 and 650 °C, as shown by infrared spectroscopy, elemental analysis, and ^{13}C and ^{29}Si solid-state MAS NMR spectroscopy. The polymer converts to a largely amorphous (by X-ray powder diffraction) Si_3N_4, containing isolated nanometer-sized crystals of α-Si_3N_4 and less than 2% C, on heating to 1000 °C. Further crystallization, grain growth, and reduction in C and H content occur upon additional heating to 1600 °C in N_2.

Introduction

Silicon nitride is an advanced structural ceramic and dielectric with applications in high-temperature environments and in electronics. Si_3N_4 powders are commonly prepared by the following methods: (1) direct nitridation of silicon from 1100 to 1400 °C;[1,2] (2) carbothermal re-

† Department of Materials Engineering, RPI.
‡ Colorado State University.
§ Department of Chemistry, RPI.

(1) Messier, D. R.; Croft, W. J. In *Preparation and Properties of Solid State Materials*; Wilcox, W. R., Ed.; Marcel Dekker: New York, 1982; Vol. 7, Chapter 2.

0897-4756/92/2804-0937$03.00/0